This is a preprint, the final version is subject to change, of the American Mineralogist (MSA)
Cite as Authors (Year) Title. American Mineralogist, in press.
DOI: https://doi.org/10.2138/am-2020-7275

Revision 1

Transjordanite, Ni_2P, a new terrestrial and meteoritic phosphide, and natural solid solutions barringerite-transjordanite (hexagonal Fe_2P–Ni_2P)

Sergey N. Britvin[1,2]*, Michail N. Murashko[1], Ye. Vapnik[3], Yury S. Polekhovsky[1†], Sergey V. Krivovichev[2,1], Maria G. Krzhizhanovskaya[1], Oleg S. Vereshchagin[1], Vladimir V. Shilovskikh[1,4], and Natalia S. Vlasenko[1]

[1]St. Petersburg State University, Universitetskaya Nab. 7/9, 199034 St. Petersburg, Russia

[2]Kola Science Center, Russian Academy of Sciences, Fersman Str. 14, 184200 Apatity, Russia

[3]Department of Geological and Environmental Sciences, Ben-Gurion University of the Negev, P.O.B. 653, Beer-Sheva 84105, Israel

[4]Institute of Mineralogy, Urals Branch of Russian Academy of Science, Miass 456317, Russia

†Deceased: September 29, 2018.

Abstract

This paper is a first detailed report of natural hexagonal solid solutions along the join Fe_2P–Ni_2P. Transjordanite, Ni_2P, a Ni-dominant counterpart of barringerite (a low-pressure polymorph of Fe_2P), is a new mineral. It was discovered in the pyrometamorphic phosphide assemblages of the Hatrurim Formation (the Dead Sea area, Southern Levant) and was named for the occurrence on the Transjordan Plateau, West Jordan. Later on, the mineral was confirmed in the Cambria meteorite (iron ungrouped, fine octahedrite) and it likely occurs in CM2 carbonaceous chondrites (Mighei group). In reflected light, transjordanite is white with a beige tint. It is non-pleochroic and weakly anisotropic. Reflectance values for four COM recommended wavelengths are [R_{max}/R_{min}, % (λ, nm)]: 45.1/44.2 (470), 49.9/48.5 (546), 52.1/50.3 (589), 54.3/52.1 (650). Transjordanite is hexagonal, space group $P\bar{6}2m$; unit cell parameters for the holotype specimen, $(Ni_{1.72}Fe_{0.27})_{1.99}P_{1.02}$, are a 5.8897(3), c 3.3547(2) Å, V 100.78(1) Å^3, Z = 3. D_{calc} = 7.30 g/cm^3. Crystal structure of holotype

transjordanite was solved and refined to $R_1 = 0.013$ based on 190 independent observed [$I > 2\sigma(I)$] reflections. The crystal structure represents a framework composed of two types of infinite rods propagated along the *c*-axis: (1) edge-sharing tetrahedra [$M(1)P_4$] and (2) edge-sharing [$M(2)P_5$] square pyramids. Determination of unit-cell parameters for 12 members of the Fe_2P–Ni_2P solid solution demonstrates that substitution of Ni for Fe in transjordanite and *vice versa* in barringerite does not obey Vegard's law, indicative of preferential incorporation of minor substituent into $M(1)$ position. Terrestrial transjordanite may contain up to 3 wt. % Mo whereas meteoritic mineral bears up to 0.2 wt. % S.

Keywords: transjordanite, barringerite, phosphide, Fe-Ni-P system, Fe_2P, Ni_2P, crystal structure, phase transitions, solid solution, Vegard's law, pyrometamorphism, meteorite, prebiotic phosphorylation

Introduction

Phase relationships in the system Fe-Ni-P play a significant role in crystallization pathways of metal-rich celestial bodies whose fragments are delivered as the iron and stony-iron meteorites (Buchwald 1975; Goldstein et al. 2009). Iron-nickel phosphides are considered to be a reservoir for reduced phosphorus in deep planetary interiors (Dera et al. 2008; Minin et al. 2018; He et al. 2019) and a source of low-valent phosphorus in the prebiotic phosphorylation processes on early Earth (Pasek et al. 2017; Gibard et al. 2019). Barringerite, $(Fe,Ni)_2P$, was the second phosphide discovered in nature (Buseck 1969), and is the next typical phosphide mineral following the schreibersite–nickelphosphide series, Fe_3P–Ni_3P (Buchwald 1975; Britvin et al. 1999). Extraterrestrial barringerite was described from several meteorite groups, including pallasites (Buseck 1969; Zucchini et al. 2018), irons (Anthony et al. 1995), howardites (Nazarov et al. 1994, Gounelle et al. 2003), carbonaceous chondrites (Mikouchi et al. 2006; Nazarov et al. 2009), and in Lunar basaltic-

anorthositic breccia Yamato 793274 (Brandstätter et al. 1991). The occurrence of barringerite on Earth is sometimes considered as a signature of extraterrestrial component (indication of impact event) (Drake et al. 2018), though its finding in garnet peridotite (Yang et al. 2005) has an obvious terrestrial origin whereas barringerite from burnt coal dumps was formed under anthropogenic influence (Bariand et al., 1977; Pierrot et al. 1977; Yao 2003). Barringerite grains recovered from heavy placer concentrates (Eremenko et al. 1974; Chen et al. 1983) are of debatable (probably meteoritic) origin. Ni-dominant members of Ni_2P–Fe_2P series were reported from two Mighei-type (CM2) carbonaceous chondrites, Boriskino and Allan Hills 83100 (Nazarov et al. 2009).

It is noteworthy that the compound Fe_2P may crystallize in two polymorphic modifications: the low-pressure (LP) hexagonal one having barringerite (LP-Fe_2P) structure (Rundquist and Jellinek 1959), and the high-pressure (HP, > 8 GPa) orthorhombic polymorph which adopts Co_2Si structure type (Sénateur et al. 1976; Dera et al. 2008). Synthetic Ni_2P has a barringerite-type LP structure to at least 50 GPa (Dera et al. 2009). Natural high-pressure $(Fe,Ni)_2P$, allabogdanite, was discovered in a small iron meteorite Onello (Britvin et al. 2002) and was recently confirmed in two other irons belonging to the same Ni-rich ataxite group: Barbianello and Santa Catharina (Britvin et al. 2019b). The discovery of allabogdanite raises a question of proper (either LP or HP) diagnostic of natural, in particular meteoritic, $(Fe,Ni)_2P$ minerals, as there is only one meteoritic barringerite (Buseck 1969) whose structural attribution was validated using an X-ray diffraction.

Barringerite is the most abundant phosphide mineral among terrestrial phosphide associations recently reported in a pyrometamorphic suite of the Hatrurim Formation, in the vicinity of the Dead Sea (in Israel and West Jordan) (Britvin et al. 2015, 2017b). During the ongoing research of those phosphide assemblages, we found that a complete series of solid solutions between barringerite-type polymorphs of Fe_2P and Ni_2P does exist in nature. The Ni-dominant member of the series, a new mineral, was named transjordanite, for the type locality on the Transjordan Plateau in West Jordan. Both the mineral and its name have been approved by the IMA Commission on New

Minerals, Nomenclature and Classification (IMA 2013–106). The holotype specimen of transjordanite is deposited at the Mineralogical Museum of the Department of Mineralogy, Saint Petersburg State University, St. Petersburg, Russia, catalogue number 19605. In the course of an investigation of meteoritic phosphide assemblages from a collection of the Mining Museum, Saint Petersburg Mining Institute (Britvin 2007), an interesting association of Fe_2P–Ni_2P minerals was revealed in the Cambria iron meteorite (fine octahedrite). Recent re-examination had showed that this assemblage contains Ni-dominant analogue of barringerite and thus comprises the first confirmed extraterrestrial occurrence of transjordanite. Whereas synthetic compounds along the join Fe_2P–Ni_2P are well studied owing to their promising magnetic properties (e.g., Zach et al. 2004; Balli et al. 2007), wear resistance (Sudagar et al. 2013) and catalytic applications (Hitihami-Mudiyanselage et al. 2015; Wexler et al. 2016), the majority of Fe_2P–Ni_2P minerals have no characterization except of electron microprobe data. We herein provide a detailed report on naturally occurring transjordanite and its solid solutions with barringerite, in comparison with the reported data on their synthetic analogues.

Occurrence of transjordanite

The Hatrurim Formation, otherwise known as the Mottled Zone, has attracted significant mineralogical interest during the past decades. This is the world's largest, geologically juvenile suite of pyrometamorphic rocks whose outcrops are scattered over the area ~30,000 km^2 across the territory of Israel, Palestinian Authority and West Jordan. The description of geological setting and mineral assemblages of the Mottled Zone is given in a series of papers (Gross 1977; Burg et al. 1999; Vapnik et al. 2007; Geller et al. 2012; Novikov et al. 2013; Kolodny et al. 2014; Sokol et al. 2019). Phosphide assemblages of the Mottled Zone represent super-reduced part of its mineralogy (Britvin et al. 2015). The minerals related to barringerite-transjordanite series are the most abundant phosphides of the Mottled Zone, found both on Israel and Jordan shoulders of this formation.

Transjordanite from Jordan, including the holotype specimen, comes from the small phosphorite quarry in West Jordan (31° 21' 52" N, 36° 10' 55" E) which crops out the so-called "paralavas" of the Daba-Siwaqa complex. Paralavas comprise Cretaceous-Tertiary sediments (chalks and marls) melted at the temperature beyond 1100 °C, yielding different types of remelted basic silicate rocks. Phosphides, including minerals of transjordanite-barringerite series, are commonly confined to the interstices between calcined unmelted sediments and paralavas (Britvin et al. 2015). In the Hatrurim Basin (located a few km west of the southern subbasin of the Dead Sea, Israel), transjordanite was found in an unusual diopside microbreccia occurred in the midstream of the Nahal Halamish (Halamish wadi).

Cambria is a 16 kg iron meteorite found in 1818 nearby Lockport, Niagara County, New York, U.S.A., 43° 12' N, 78° 49' W. It belongs to a group of fine octahedrites (10.4 wt. % Ni) and is chemically classified as an ungrouped (anomalous) iron. A detailed description of the meteorite along with a review of early references is given by Buchwald (1975) who emphasizes that Cambria is a unique iron which apparently underwent a violent (perhaps shock-induced) event during its escape from the parent body. A characteristic feature of Cambria is its enrichment in troilite whose millimeter- to centimeter-sized nodules constitute up to 8 % of a surface of meteorite slices (Buchwald 1975). At the interface with encasing "kamacite" (Ni-rich variety of α-iron), troilite nodules are encrusted with millimeter-thick rims of brecciated schreibersite. A few millimeter-sized chips of troilite-phosphide assemblages were extracted for the study from the Cambria specimen M9/1 stored in the Mining Museum, Saint Petersburg Mining Institute (Britvin 2007).

Appearance and mineral associations

Terrestrial transjordanite from the Hatrurim Formation appears as irregular grains reaching 0.2 mm in size which are disseminated in a matrix of altered diopside microbreccia (Fig. 1). The mineral is frequently corroded and replaced by the rims of polycrystalline murashkoite, FeP (Britvin et al.

2019c) (Fig. 1A, B). Associated phosphides may also include zuktamrurite, FeP_2, negevite, NiP_2, and halamishite, Ni_5P_4 (Britvin et al. 2015, 2019a) whereas sulfides comprise pyrrhotite (Fig. 2A, B) and troilite. Other associated minerals are represented by hematite, magnetite, Cu-bearing trevorite, merrillite-like phosphate, and an intimate mixture of undefined phosphates and hydrous silicates (Fig. 1, Table S1). Late hydrothermal (or possibly, supergene) calcite fills up the interstices and fractures between phosphide-bearing assemblages. Transjordanite grains which compositionally approach Ni_2P end-member (Fig. 1C, D, Table 1) may contain molybdenite (exsolution?) lamellae cross-cutting the host transjordanite matrix. Molybdenite, in due course, is commonly replaced by powdery pseudomorphs of unidentified Ca molybdate (Fig. 1D, Table S1).

Mineral association of meteoritic transjordanite is completely different from that of terrestrial one. The examined sections of the Cambria meteorite are composed of recrystallized microgranular troilite (10-20 μm grain size) stuffed with fragments of finely brecciated schreibersite (Fig. 2A). Schreibersite grains are cleaved by numerous shear fractures which are infilled with troilite. Both minerals show no signs of alteration along their interfaces, besides of partial replacement of troilite with supergene Fe-oxides. However, the smaller (less than 100 μm) schreibersite fragments dispersed in troilite are frequently encrusted with 5-10 μm-thick, onion-like rims composed of submicrocrystalline transjordanite-barringerite aggregate (Fig. 2B, C) where the grain size could not be resolved using the SEM employed for imaging purposes (apparently less than 0.5 μm). It is noteworthy that the overall structure of phosphide-troilite assemblages found in the Cambria octahedrite almost entirely replicates the structure of schreibersite-barringerite-troilite interfaces described in the Ollague pallasite – the type meteorite where barringerite was discovered as a new mineral (Buseck 1969). Because Cambria and Ollague belong to different meteorite groups, the obvious similarity of their phosphide-troilite assemblages might provide some insights into post-formation thermal history of these meteorites which is discussed in concluding chapters.

151

152 **Analytical methods**

153 Examination of the minerals under reflected light was carried out in rock sections embedded into
154 epoxy resin and polished using conventional preparation techniques. Reflectance values were
155 measured by means of a MSF-21 spectrophotometer (LOMO Company, St. Petersburg) using WTiC
156 as a reflectance standard, monochromator slit of 0.4 mm with beam diameter of 0.1 mm. The
157 Vicker's hardness was measured with PMT-3 microhardness tester (LOMO) under 20 g load.
158 Energy-dispersive (EDX) compositional screening and elemental mapping was performed on
159 carbon-coated sections using an Oxford Instruments AzTec Energy X-Max 20 spectrometer attached
160 to a Hitachi S-3400N scanning electron microscope (SEM) operated at 20 kV accelerating voltage
161 and 1 nA beam current. Electron microprobe data for selected grains (Tables 1 and 2) were obtained
162 by means of an INCA WAVE 500 wavelength-dispersive (WDX) spectrometer attached to the same
163 SEM under 20 kV accelerating voltage and 15 nA beam current, 2 μm beam size, 20 s peak counting
164 time, 10 s background counting time. The following standareds were used: GaP (P*K*α), pyrite (Fe*K*α,
165 S*K*α), metallic Cr (Cr*K*α), Co (Co*K*α), Ni (Ni*K*α), and Mo (Mo*L*α). Phosphide grains selected for X-
166 ray diffraction studies were hand-picked from the polished sections. Powder X-ray diffraction
167 (PXRD) study was carried out by means of a Rigaku RAXIS Rapid II diffractometer equipped with
168 a curved (semi-cylindrical) imaging plate (Debye-Scherrer geometry, r = 127.4 mm) and Co*K*α-
169 radiation source (rotating anode, 40 kV, 15 mA), with Rigaku VariMax microfocus mirror optics. In
170 order to achieve a better measurement accuracy, the imaging plate was calibrated against NIST Si
171 640e standard. PXRD data aimed at determination of unit-cell parameters were acquired from
172 undestroyed phosphide grains using a Gandolfi technique implemented in a Rigaku RAXIS Rapid II
173 diffractometer (see above). PXRD patterns of the holotype specimen and of the mineral from the
174 Cambria meteorite (Table S2) were obtained on powdered micro-spherical samples. Imaging plate-
175 to-profile data conversion was performed using osc2xrd software (Britvin et al. 2017b). Unit-cell

refinements were carried out by Pawley full pattern decomposition (Pawley 1981) implemented in a Bruker Topas v. 5.0 software (Bruker 2014). The deviations of parameters determination was estimated by comparison of several testing duplicate datasets and was found to be ±0.0002 Å for *a* parameter and ±0.0001 Å for *c* parameter. Calculation of PXRD pattern for a holotype transjordanite (Table S2) was performed by means of a Stoe WinXPOW v. 2.08 software (Stoe 2003), taking atomic coordinates determined by the structure refinement from a single crystal and unit-cell parameters refined from powder diffraction data. X-ray single-crystal data collection for the holotype crystal of transjordanite was carried out by means of a Bruker Kappa APEX DUO diffractometer equipped with a microfocus Mo*K*α-radiation source. A hemisphere of reciprocal space was collected using φ- and ω-scans at the frame width of 1 °. Data collection and integration procedures (Table 3) were completed with Bruker APEX2 and SAINT software (Bruker 2003). Crystal structure was solved by a dual space method and refined to $R_1 = 0.013$ by means of a *SHELX*-2014 software (Sheldrick 2015) incorporated into Olex2 program environment (Dolomanov et al. 2009). Full structural data on holotype transjordanite can be retrieved from the Crystallographic Information File (CIF) deposited in the Supplemental Data.

Physical properties

Terrestrial transjordanite from the Hatrurim Formation possesses grayish-white color under binocular and has a bright metallic luster. Transjordanite-barringerite aggregates from the Cambria meteorite exhibit gray color. In powdery state, the mineral is gray. In reflected light, transjordanite is white with beige tint. It is weakly bireflectant ($\Delta R = 1.8$ % at 589 nm), non-pleochroic and weakly anisotropic. Reflectance values for the holotype specimen (analysis T03 in Table 1) are given in Table S3. Microhardness measured for a grain from the Hatrurim Basin (analysis H04 in Table 1) is 658 kg/mm^2 (average of 3 indentations). Transjordanite containing up to ~95 mol. % Ni_2P is brittle.

However, upon further approaching Ni_2P end-member (Fig. 1C,D; Table 1), the mineral becomes ductile. The ductility of synthetic Ni_2P end-member was mentioned by Rundqvist (1962).

The densities calculated for nine Mo-free members of barringerite-transjordanite series exhibit quasi-linear dependence on Fe/Ni ratio (Fig. 3) which is consistent with the oppositely directed change of their *a* and *c* unit-cell parameters (Table S4). The obtained density values well coincide with the reference data reported for synthetic Fe_2P, Ni_2P and $(Fe_{1.00}Ni_{1.00})_{\Sigma=2.00}P$ (Fruchart et al. 1969). Four terrestrial Mo-bearing barringerite-transjordanite members (Table 1) demonstrate an expected systematic increase of calculated density relative to Mo-free Fe_2P–Ni_2P solid solutions (Table S4, Fig. 3). In spite of a decreased accuracy of unit-cell parameters reported for barringerite from the Ollague pallasite (Buseck 1969), its density also well fits to a general compositional trend.

Qualitative testing of magnetic properties of barringerite-transjordanite grains under ambient conditions showed that they are non-ferromagnetic. This observation is consistent with the previously reported results for synthetic Fe_2P–Ni_2P solid solutions which exhibit the maximum value of the Curie point at 342 K (69 °C) and 0.16 Ni *apfu*, with an abrupt decrease of ferro- to paramagnetic transition temperature upon departure from this point (Fruchart et al. 1969; Fujii et al. 1978).

Chemical composition

Hatrurim Formation. EDX screening of more than 200 phosphide-bearing assemblages from both Israel and West Jordan showed that there exists a complete series of natural solid solutions between Fe_2P (barringerite) and Ni_2P (transjordanite) end-members (Fig. 4). An important characteristic of these minerals is their intragrain compositional homogeneity – we did never observe chemical zoning across the dozens of studied grains. At the same time, several neighboring grains within an area of 5×5 mm^2 may differ in grain-to-grain composition from 0.07 to 1.97 Ni *apfu* (atoms per formula unit). A peculiar feature of terrestrial barringerite-transjordanite minerals is that they

frequently contain noticeable amounts of Mo (up to 3 wt. %) (Fig. 4, Table 1). Chromium and vanadium which were sporadically detected in barringerite (Britvin et al. 2017b) have never been encountered in transjordanite. The Co content in transjordanite is generally insignificant and sometimes falls beyond detection limit of WDX analysis (less than ~0.05 wt. %) (Table 1). The maximum Co content of ~0.7 wt. % was so far encountered in transjordanite grain with a composition approaching Ni_2P end-member (Table 1, Fig. 1). For a crystal chemical study, an array of 12 grains was selected with the compositions having sufficiently uniform distribution along the join Fe_2P–Ni_2P (Table 1). The holotype specimen of transjordanite from West Jordan corresponding to $(Ni_{1.72}Fe_{0.27})_{\Sigma=1.99}P_{1.02}$ (analysis T03 in Table 1) was also included in this selection.

The Cambria meteorite. Barringerite-transjordanite aggregates replacing schreibersite in the Cambria octahedrite exhibit strong compositional zoning. The outer zones of contact with troilite are composed of transjordanite (max. Ni = 1.52 *apfu*) whereas inner shells adjoining schreibersite are represented by barringerite (max. Fe = 1.58 *apfu*), with a steep compositional gradient in between (Fig. 2D, 3, Table 2). The average rim composition determined from several areas corresponds to $(Fe_{1.18}Ni_{0.81}Co_{0.01})_{\Sigma=2.00}(P_{0.99}S_{0.01})_{\Sigma=1.00}$ – the formula which is remarkably close to $(Fe_{1.14}Ni_{0.83}Co_{0.01})_{\Sigma=1.98}P_{\Sigma=1.02}$ of holotype barringerite from the Ollague pallasite (Buseck 1969). Meanwhile, the composition of schreibersite, $(Fe,Ni)_3P$, which is a primary mineral relative to transjordanite-barringerite in Cambria (Fig. 2), is rather uniform from grain to grain. Schreibersite from Cambria has the atomic ratio Ni/(ΣFeNiCo) = 0.27 (Table 2) which is substantially different from that of schreibersite from Ollague having Ni/(ΣFeNiCo) = 0.36 (Buseck 1969). Almost all analyses of transjordanite-barringerite aggregates from Cambria show some content of sulfur (Fig. 2D, 4; Table 2). In this respect, they resemble sulfur-bearing Fe_2P–Ni_2P minerals from CM2 carbonaceous chondrites (Nazarov et al. 2009).

Powder X-ray diffraction (PXRD) and crystal structure

PXRD analysis aimed at determining the unit-cell parameters (Table S4) was carried out on 12 grains of terrestrial transjordanite-barringerite whose chemical compositions are given in Table 1. Full PXRD data for a powdered sample of holotype transjordanite (analysis T03 in Table 1) and the Gandolfi data for transjordanite having the maximum Ni content (analysis H01) are given in Table S2. PXRD pattern of the mineral from the Cambria meteorite (Table S2) was obtained from an averaged powder sample comprising a continuous series of Fe_2P–Ni_2P solid solutions (*cf*. Fig. 4). In spite that it thus represents averaged values of *d*-spacings, it is unambiguously indexed in hexagonal (barringerite) setting, confirming its relation to barringerite structure type. Figure 5 shows the plots describing the dependence between unit-cell parameters of terrestrial transjordanite-barringerite minerals and their Ni content. Both *a* and *c* parameter curves exhibit complex, S-shaped dependencies which strongly violate Vegard's law (Zen 1956; Denton and Ashcroft 1991). At the same time, these profiles are consistent with the data by Fruchart et al. (1969) for the synthetic Ni_2P–Fe_2P compounds compositionally equilibrated at 850–900 °C (the blue plots on Fig. 5). The comparison of both datasets shows that the unit-cell parameters of the minerals are equal or larger than the corresponding values of their synthetic analogues. The latter evidences for a perfect M_2P stoichiometry of examined minerals because deviations from the ideal M_2P composition (caused by vacancies on the metal sites) would result in a significant (up to 0.1 Å) decrease of unit-cell parameters (Carlsson et al. 1973).

Vegard's law (Zen 1956; Denton and Ashcroft 1991) postulates a linear change of unit-cell parameters across a given series of solid solutions, provided that the substituting elements randomly occupy the permitted positions in the structure. Strong deviations from Vegard's law indicate a selective incorporation of substituting element into preferred structural positions, as it can be exemplified by the schreibersite–nickelphosphide series, Fe_3P–Ni_3P (Skála and Císařová 2005). The crystal structure of transjordanite (Fe_2P structure type, Table 4) bears two independent metal sites. The metal atom at *M*(1) position is coordinated by four P atoms forming a distorted tetrahedron

[MP$_4$] (Fig. 6). The metal occupying M(2) site is bonded to five P atoms in [MP$_5$] square-pyramidal coordination (Table 3). The whole structure can be expressed as an interleaved sequence of two types of infinite rods propagating along the *c* axis (Fig. 6). The first rod type is composed of corner-sharing [M(1)P$_4$] tetrahedra alternating with the empty square pyramids [□P$_5$]. The next type of rods is built up of edge-sharing [M(2)P$_5$] square pyramids alternating with the empty tetrahedra [□P$_4$]. The rods are arranged into a framework *via* common P–P edges of adjacent metal-phosphorus polyhedra. The combination of two metal-centered and two empty polyhedra can be expressed as a rhombohedral supercell highlighted on Fig. 6B (Fruchart et al. 1969). A study of Fe/Ni distribution between M(1) and M(2) sites by means of Mössbauer spectroscopy (Maeda and Takashima 1973) revealed rather unusual behavior of substituting metal: the substituent (either Fe into Ni$_2$P or Ni into Fe$_2$P) begins to incorporate exclusively into M(1) (tetrahedral) site until reaching a limit of about 30 mol. % (0.6 *apfu*). Then the substitution continues almost randomly into M(1) and M(2) sites. Such a behavior readily explains the observed S-shaped profile of cell parameters *vs.* composition dependence plot (Sénateur et al. 1977). The knowledge of Fe/Ni substitution behavior allowed selection of a proper approach to refinement of site occupancies in the crystal structure of natural transjordanite. Upon testing of a free refinement of M(1) and M(2) site occupancies, the crystal structure of holotype transjordanite was finally refined with Fe being entirely incorporated into M(1) position (Table 4). The refined M(1) site occupancy was found to be (Ni$_{0.86}$Fe$_{0.14}$), in an excellent agreement with the formula (Ni$_{1.72}$Fe$_{0.27}$)$_{\Sigma=1.99}$P$_{1.02}$ derived from electron microprobe data.

Origin of the barringerite-transjordanite series minerals

Hatrurim Formation. The intragrain homogeneity of terrestrial barringerite-transjordanite, their perfect M_2P stoichiometry and Fe/Ni ordering suggest that these minerals were annealed in the solid state at the temperature permitting Fe/Ni diffusion processes. Based on the experiments on synthetic Fe$_2$P–Ni$_2$P system, one can suggest that the annealing temperature was not lower than 850–900 °C

(Fruchart et al. 1969). Fe_2P and Ni_2P melt congruently at 1370 and 1105 °C, respectively (Schmetterer et al. 2009; Okamoto 1990), hence phosphide crystallization and metal ordering could occur in the range between 850 and 1370 °C, i.e., either in the melted or solidified paralava (Vapnik et al. 2007). Phosphides could be equally formed by reduction of merrillite-type phosphates found in the same assemblages (Fig. 1, Table S1) or by gas-phase transport reactions involving phosphine and volatile metal-carbonyl complexes (Britvin et al. 2015). The latter mechanism can also be applied for explanation of high Ni and Mo content confined to phosphide minerals (Table 1, Fig. 4).

Meteoritic occurrences. Contrary to terrestrial mineral series, barringerite-transjordanite assemblages in Cambria exhibit strong chemical heterogeneity. At the same time, the adjacent relict schreibersite grains have rather uniform composition (Table 2, Fig. 2C, D). The various scenarios can be proposed for explanation of the emergence of the observed assemblages. The most straightforward one relies upon post-formational thermal history of both Ollague and Cambria meteorites. The Ollague pallasite was shown to be an artificially reheated fragment of the Imilac meteorite. It was suggested that barringerite in Ollague might represent a product of reaction between schreibersite and troilite during the annealing process (Buchwald 1976). Although Cambria did not undergo artificial treatment, it was severely ablated during penetration of the Earth's atmosphere (Buchwald 1975). Troilite nodules in Cambria are confined to a peripheral zone of the meteorite, and they were heavily annealed during ablation process (Buchwald 1975). In that case, the emergence of barringerite-transjordanite rims in Cambria could be explained by natural thermal annealing. However, the replacement of M_3P phosphide (schreibersite) by M_2P one (barringerite-transjordanite) would require an infusion of phosphorus into the system or removal of the metal from there. Therefore, taking into account short annealing time, the question persists concerning a chemical balance budget in the closed system.

The second possible scenario implies the formation of barringerite-transjordanite rims by replacement (or overgrowth) of schreibersite at a temperature below "freezing" of diffusion

processes in the Fe–Ni–P system, i.e., below 300 °C (Romig and Goldstein 1980). This could be accomplished after the completion of nebular condensation of schreibersite (Lodders 2003), but prior to accretion of troilite nodules, according to a scheme: $2(Fe,Ni)_3P$ (solid) + P (vapor) → $3(Fe,Ni)_2P$ (solid). This hypothesis places phosphide assemblages of Cambria and pallasites (Buseck 1969; Zucchini et al. 2018) inline with the phosphides of carbonaceous chondrites (Gounelle et al. 2003; Nazarov et al. 2009). A substantial argument supporting this point of view is noticeable sulfur content encountered in M_2P phosphides from Cambria (Table 2, Fig. 4) and CM2 chondrites (Nazarov et al. 2009).

One more hypothesis which is amongst those introduced by Buseck (1969) implies that barringerite in the Ollague pallasite (and thus in Cambria as well) can be a product of terrestrial weathering of schreibersite. This assumption is supported by the widespread industrial use of electroless Ni phosphides deposition in aquatic environment (Sudagar et al. 2013) and by finding of natural schreibersite formed at the deep-sea conditions (Borodaev et al. 1982). This interesting point of view readily explains the enrichment of barringerite-transjordanite in Ni, relative to schreibersite. In the meteorites, the $M_3P \rightarrow M_2P$ replacement process would be accompanied by partial oxidation of phosphidic Fe to Fe^{3+}. The latter would precipitate in the form of iron hydroxides along the troilite-phosphide interfaces (Fig. 2). Such a process would be of great importance for elucidation of prebiotic phosphorylation pathways (Pasek et al. 2017; Kitadai and Maruyama 2018). It is not clear, however, why such a replacement has never been encountered among weathered troilite-schreibersite assemblages which are ubiquitous in iron and stony-iron meteorites (Buchwald 1975).

Implications

The importance of study of natural Fe_2P–Ni_2P solid solutions relies upon their relation to the Fe-Ni-P system which is, along with the Fe-Ni-S and Fe-Ni-C ternaries, belongs to the most significant reduced cosmochemical systems. The knowledge of phase relationships and compositional

variations of Fe-Ni phosphide minerals has a broad range of implications, including the origin of Solar System, composition of deep planetary interiors, meteoritics, terrestrial processes in super-reduced environments, and processes of prebiotic phosphorylation occurred on early Earth.

Acknowledgments

The authors gratefully acknowledge the curators of the Mining Museum, St. Petersburg Mining Institute, for providing the sample of the Cambria meteorite. We are thankful to the Associate Editor, Giacomo Diego Gatta, two anonymous Referees and the technical Editor who contributed to significantly improve the quality of the manuscript.

This research was funded by Russian Science Foundation, grant 18-17-00079. The authors thank X-ray Diffraction Centre, "Geomodel" Resource Centre and Nanophotonics Resoure Centre of St. Petersburg State University for providing instrumental and computational resources.

References cited

Anthony, J.W., Bideaux, R.A., Bladh, K.W., and Nichols, M.C. (1995) Handbook of Mineralogy, vol. 3. Mineral Data Publishing House, Tucson, AZ, p 44.

Balli, M., Fruchart, D., Gignoux, D., Tobola, J., Hlil, E.K., Wolfers, P., and Zach, R. (2007) Magnetocaloric effect in ternary metal phosphides $(Fe_{1-x}Ni_x)_2P$. Journal of Magnetism and Magnetic Materials, 316, 358–360.

Bariand, P., Cesbron, F., and Geffroy, J. (1977) Les minéraux, leurs gisements, leurs associations. Editions Minéraux et Fossiles. Bureau de Recherches Géologiques et Minières (France), 489 p (in French).

373 Borodaev, Yu.S., Bogdanov, Yu.A., and Vyalsov, L.N. (1982) New nickel-free variety of
374 schreibersite Fe_3P, Zapiski Rossiiskogo Mineralogicheskogo Obshchestva, 111(6), 682–687
375 (in Russian).
376 Brandstätter, F., Koeberl, C., and Kurat, G. (1991) The discovery of iron barringerite in lunar
377 meteorite Y-793274. Geochimica et Cosmochimica Acta, 55, 1173–1174 .
378 Britvin, S. N. (2007) Phosphides in metal-rich meteorites. Ph.D. Thesis, Saint Petersburg State
379 University, 203 p.
380 Britvin, S.N., Kolomensky, V.D., Boldyreva, M.M., Bogdanova, A.N., Kretser, Yu.L., Boldyreva,
381 O.N., and Rudashevskii, N.S. (1999) Nickelphosphide, $(Ni,Fe)_3P$, the nickel analog of
382 schreibersite. Zapiski Vsesoyuznogo Mineralogicheskogo Obshchestva, 128, 64–72 (in
383 Russian).
384 Britvin, S.N., Murashko, M.N., Vapnik, Ye., Polekhovsky, Yu.S., and Krivovichev, S.V. (2015)
385 Earth's phosphides in Levant and insights into the source of Archaean prebiotic phosphorus.
386 Scientific Reports, 5, 8355.
387 Britvin, S.N., Dolivo-Dobrovolsky, D.V., and Krzhizhanovskaya, M.G. (2017a) Software for
388 processing the X-ray powder diffraction data obtained from the curved image plate detector of
389 Rigaku RAXIS Rapid II diffractometer. Zapiski Rossiiskogo Mineralogicheskogo
390 Obshchestva, 146, 104–107.
391 Britvin, S.N., Murashko, M.N., Vapnik, E., Polekhovsky, Yu.S., Krivovichev, S.V. (2017b)
392 Barringerite Fe_2P from pyrometamorphic rocks of the Hatrurim Formation, Israel. Geology of
393 Ore Deposits, 59, 619–625.
394 Britvin, S.N., Murashko, M.N., Vapnik, Ye., Polekhovsky, Yu.S., Krivovichev, S.V., Vereshchagin,
395 O.S., Vlasenko, N.S., Shilovskikh, V.V., and Zaitsev, A.N. (2019a) Zuktamrurite, FeP_2, a new
396 mineral, the phosphide analogue of löllingite, $FeAs_2$. Physics and Chemistry of Minerals, 46,
397 361–369.

Britvin, S.N., Rudashevsky, N.S., Krivovichev, S.V., Burns, P.C., and Polekhovsky, Y.S. (2002) Allabogdanite, $(Fe,Ni)_2P$, a new mineral from the Onello meteorite: The occurrence and crystal structure. American Mineralogist, 87, 1245–1249.

Britvin S.N., Shilovskikh, V.V., Pagano, R., Vlasenko, N.S., Zaitsev, A.N., Krzhizhanovskaya, M.G., Lozhkin, M.S., Zolotarev, A.A., and Gurzhiy, V.V. (2019b) Allabogdanite, the high-pressure polymorph of $(Fe,Ni)_2P$, a stishovite-grade indicator of impact processes in the Fe–Ni–P system. Scientific Reports, 9, 1047.

Britvin, S.N., Vapnik, Ye., Polekhovsky, Yu.S., Krivovichev, S.V., Krzhizhanovkaya M.G., Gorelova, L.A., Vereshchagin, O.S., Shilovskikh, V.V., and Zaitsev, A.N. (2019c) Murashkoite, FeP, a new terrestrial phosphide from pyrometamorphic rocks of the Hatrurim Formation, Southern Levant. Mineralogy and Petrology, 113, 237–248.

Bruker (2003) SAINT (ver. 7.60A). Bruker AXS Inc., Madison, Wisconsin, USA.

Bruker (2014). Topas 5.0. General profile and structure analysis software for powder diffraction data. Karlsruhe, Germany.

Buchwald, V.F. (1975) Handbook of iron meteorites. University of California Press, Berkeley, Los Angeles, London.

Buchwald, V.F. (1976) The mineralogy of iron meteorites. Phylosophical Transactions of the Royal Society A, 286, 453–491.

Burg, A., Kolodny, Ye., and Lyakhovsky, V. (1999) Hatrurim - 2000: The "Mottled Zone" revisited, forty years later. Israel Journal of Earth Sciences, 48, 209–223.

Buseck, P.R. (1969) Phosphide from meteorites: Barringerite, a new iron-nickel mineral. Science, 165, 169–171.

Carlsson, B., Goelin, M., and Rundqvist, S. (1973) Determination of the homogeneity range and refinement of the crystal structure of Fe_2P. Journal of Solid State Chemistry, 8, 57–67.

Chen, K., Jin, Z., and Peng, Z. (1983) The discovery of iron barringerite (Fe_2P) in China. Dizhi Kexue, 127–135 (in Chinese with English abstract).

Denton, A.R., and Ashcroft, N.W. (1991) Vegard's law. Physical Review A, 43, 3161–3164.

Dera, P., Lavina, B., Borkowski, L.A., Prakapenka, V.B., Sutton, S.R., Rivers, M.L., Downs, R.T., Boctor, N.Z., and Prewitt, C.T. (2008) High-pressure polymorphism of Fe_2P and its implications for meteorites and Earth's core. Geophysical Research Letters, 35, L10301.

Dera, P., Lavina, B., Borkowski, L. A., Prakapenka, V. B., Sutton, S. R., Rivers, M. L., Downs, R. T., Boctor, N. Z., and Prewitt, C. T. (2009) Structure and behavior of the barringerite Ni end-member, Ni_2P, at deep Earth conditions and implications for natural Fe-Ni phosphides in planetary cores. Journal of Geophysical Research, 114, B03201.

Dolomanov, O.V., Bourhis, L.J., Gildea, R.J., Howard, J.A., and Puschmann, H. (2009) OLEX2: a complete structure solution, refinement and analysis program. Journal of Applied Crystallography, 42, 339–341.

Drake, S.M., Beard, A.D., Jones, A.P., Brown, D.J., Dominic Fortes, A., Millar, I. L., Andrew Carter, A., Baca, J., and Downes, H. (2018) Discovery of a meteoritic ejecta layer containing unmelted impactor fragments at the base of Paleocene lavas, Isle of Skye, Scotland. Geology, 46, 171–174.

Eremenko, G.K., Polkanov, Yu.A., and Gevork'yan, V.Kh. (1974) Cosmogenic minerals in the Poltava deposits of the Konka–Yalynsk depression in northern Azov Region. Mineralogiya Osadochnih Obrazovaniy, 1, 66–76 (in Russian).

Fruchart, R., Roger, A., and Sénateur, J.P. (1969) Crystallographic and Magnetic Properties of Solid Solutions of the Phosphides M_2P, M = Cr, Mn, Fe, Co, and Ni. Journal of Applied Physics, 40, 1250–1257.

Fujii, H., Hōkabe, T., Fujiwara, H., and Okamoto, T. (1978) Magnetic properties of single crystals of the system $(Fe_{1-x}Ni_x)_2P$. Journal of the Physical Society of Japan, 44, 96–100.

447 Geller, Y.I., Burg, A., Halicz, L., and Kolodny, Y. (2012) System closure during the combustion
448 metamorphic ”Mottled Zone” event, Israel. Chemical Geology, 334, 25–36.
449 Gibard, C., Gorrell, I.B., Jimenez, E.I., Kee, T.P., Pasek, M.A., and Krishnamurthy, R. (2019)
450 Geochemical Sources and Availability of Amidophosphates on the Early Earth. Angewandte
451 Chemie, International Edition, 58, 8151–8155.
452 Goldstein, J. I., Scott, E. R. D., and Chabot, N. L. (2009) Iron meteorites: Crystallization, thermal
453 history, parent bodies, and origin. Chemie der Erde – Geochemistry, 69, 293–325.
454 Gounelle, M., Zolensky, M.E., Liou, J.-C., Bland, P.A., and Alard, O. (2003) Mineralogy of
455 carbonaceous chondritic microclasts in howardites: identification of CM2 fossil
456 micrometeorites. Geochimica et Cosmochimica Acta, 67, 507–527.
457 Gross, S. (1977) The mineralogy of the Hatrurim Formation, Israel. Geological Survey of Israel
458 Bulletin, 70, 1–80.
459 He, X.-J., Guo, J.-Z., Wu, X., Huang, S.-X., Qin, F., Gu, X.-P., and Qin, S. (2019) Compressibility
460 of natural schreibersite up to 50 GPa. Physics and Chemistry of Minerals, 46, 91–99.
461 Hitihami-Mudiyanselage, A., Arachchige, M.P., Seda, T., Lawes, G., and Brock, S.L. (2015)
462 Synthesis and characterization of discrete $Fe_xNi_{2-x}P$ nanocrystals ($0 < x < 2$): compositional
463 effects on magnetic Properties. Chemistry of Materials, 27, 6592–6600.
464 Kitadai, N., and Maruyama, S. (2018) Origins of building blocks of life: A review. Geoscience
465 Frontiers, 9, 1117–1153.
466 Kolodny, Y., Burg, A., Geller, Y.I., Halicz, L., and Zakon, Y. (2014) Veins in the combusted
467 metamorphic rocks, Israel; Weathering or a retrograde event? Chemical Geology, 385, 140–
468 155.
469 Lodders, K. (2003) Solar System Abundances and Condensation Temperatures of the Elements. The
470 Astrophysical Journal, 591, 1220–1247.

Maeda, Y., and Takashima, Y. (1973) Mössbauer studies of FeNiP and related compounds. Journal of Inorganic and Nuclear chemistry, 35, 1963–1969.

Mikouchi, T., Zolensky, M., Tachikawa, O., Komatsu, M., Ivanova, M.A., Le, L., and Gounelle, M. (2006) Electron back-scatter diffraction (EBSD) analysis of two unusual minerals in carbonaceous chondrites. Lunar and Planetary Science, 37, 1855–1855.

Minin, D.A, Shatskiy, A.F., Litasov, K.D., and Ohfuji, H. (2018) The Fe–Fe_2P phase diagram at 6 GPa. High Pressure Research, 39, 50–68.

Nazarov, M.A., Brandstätter, F., and Kurat, G. (1994) P-rich sulfide, barringerite, and other phases in carbonaceous clasts of the Erevan howardite. Proceedings of 25th Lunar and Planetary Science Conference, 979–980.

Nazarov, M. A., Kurat, G., Brandstätter, F., Ntaflos, T., Chaussidon, M., and Hoppe, P. (2009) Phosphorus-bearing sulfides and their associations in CM chondrites. Petrology, 17, 101–123.

Novikov, I., Vapnik, Ye., and Safonova, I. (2013) Mud volcano origin of the Mottled Zone, Southern Levant. Geoscience Frontiers, 4, 597–619.

Okamoto, H. (1990) The Fe-P (Iron-Phosphorus) System. Bulletin of Alloy Phase Diagrams, 11, 404–412.

Pasek, M.A., Gull, M., and Herschy, B. (2017) Phosphorylation on the early earth. Chemical Geology, 475, 149–170.

Pawley, G.S. (1981) Unit-cell refinement from powder diffraction scans. Journal of Applied Crystallography, 14, 357–361.

Pierrot, R., Pulou, R., and Picot, P. (1977). Inventaire Minéralogique de la France N° 7: Aveyron. Bureau de Recherches Géologiques et Minières (France), 223 pp (in French).

Romig, A.D., and Goldstein, J.I. (1980) Determination of the Fe–Ni and Fe–Ni–P phase diagrams at low temperatures (700–300 °C). Metallurgical Transactions, 11A, 1151–1159.

Rundqvist, S. (1962) X-ray investigations of Mn_3P, Mn_2P, and Ni_2P. Acta Chemica Scandinavica, 16, 992–998.

Rundquist, S., and Jellinek, F. (1959) The structures of Ni_6Si_2B, Fe_2P and some related phases. Acta Chemica Scandinavica, 13, 425–432.

Sheldrick, G.M. (2015) Crystal structure refinement with *SHELXL*. Acta Crystallographica, C71, 3–8.

Schmetterer, C., Vizdal, J., and Ipser, H. (2009) A new investigation of the system Ni–P. Intermetallics, 17, 826–834.

Sénateur, J., Fruchart, D., Boursier, D., Rouault, A., Montreuil, J.R., and Deyris, B. (1977) Analyse des facteurs d'ordre des métaux de transition dans les phosphures et arséniures MM'P et MM'As. Journal de Physique Colloques, 38, C7-61–C7-66.

Sénateur, J. P., Rouault, A., and Fruchart, R. (1976) Etude par spectrometrie Mossbauer des transformations cristallographiques sous hautes pressions de MnFeAs et Fe_2P. Materials Research Bulletin, 11, 631–636.

Skála, R., and Císařová, I. (2005) Crystal structure of meteoritic schreibersites: determination of absolute structure. Physics and Chemistry of Minerals, 31, 721–732.

Sokol, E.V., Kokh, S.N., Sharygin, V.V., Danilovsky, V.A., Seryotkin, Yu.V., Liferovich, R., Deviatiiarova, A.S., Nigmatulina, E.N., and Karmanov, N.S. (2019) Mineralogical diversity of Ca_2SiO_4-bearing combustion metamorphic rocks in the Hatrurim Basin: implications for storage and partitioning of elements in oil shale clinkering. Minerals, 9, 465.

Stoe (2003) WinXPOW, Version 2.08, STOE & Cie GmbH, Darmstadt.

Sudagar, J., Lian, J., and Sha, W. (2013) Electroless nickel, alloy, composite and nano coatings – A critical review. Journal of Alloys and Compounds, 571, 183–204.

Vapnik, Ye., Sharygin, V.V., Sokol, E.V., and Shagam, R. (2007) Paralavas in a combustion metamorphic complex: Hatrurim Basin, Israel. The Geological Society of America, Reviews in Engineering Geology, 18, 133–153.

Wexler, R.B., Martirez, J.M.P., and Rappe, A.M. (2016) Stable phosphorus-enriched (0001) surfaces of nickel phosphides. Chemistry of Materials, 28, 5365–5372.

Yang, J.S., Bai, W.J., Rong, H., Zhang, Z.M., Xu, Z.Q., Fang, Q.S., Yang, B.G., Li, T.F., Ren, Y.F., Chen, S.Y., Hu, J.-Z., Su, J.F., and Mao, H.K. (2005) Discovery of Fe_2P alloy in garnet peridotite from the Chinese continental scientific drilling project (CCSD) main hole. Acta Petrologica Sinica, 21, 271–276.

Yao, A. (2003) Study on gangue of tonstein within no. 5 coal-bed in Hulstai Coal District, Ningxia. Northwestern Geology, 36, 78–83 (in Chinese, with English abstract).

Zach, R., Tobola, J., Sredniawa, B., Kaprzyk, S., Casado, C., Bacmann, M., and Fruchart, D. (2004) Magneto-elastic properties and electronic structure analysis of the $(Fe_{1-x}Ni_x)_2P$ system. Journal of Alloys and Compounds, 383, 322–327.

Zen, E. (1956) Validity of "Vegard's law". American Mineralogist, 41, 523–524.

Zucchini, A., Petrelli, M., Frondini, F., Petrone, C. M., Sassi, P., Di Michele, A., Palmerini, S., Trippella, O., and Busso, M. (2018) Chemical and mineralogical characterization of the Mineo (Sicily, Italy) pallasite: a unique sample. Meteoritics and Planetary Science, 53, 268–283.

List of figure captions

Figure 1. Transjordanite assemblages in the Hatrurim Formation, Southern Levant. (A) Transjordanite in a matrix of altered paralava. Transjordan Plateau, West Jordan (the type locality). Photomicrograph in reflected light. (B) The same grain, SEM BSE image. Transjordanite is corroded by rims of murashkoite, FeP. (C) Transjordanite (Ni_2P end-member) in phosphate-oxide assemblage. SEM BSE image. (D) Grain of transjordanite (H01 in Table 1) cross-cutted by altered molybdenite lamellae that are replaced by unknown hydrous Ca molybdate (Ca-Mo-O). (C) and (D): Nahal Halamish, Hatrurim basin, Israel. Abbreviations: Tj, transjordanite; Cal, calcite; Di, diopside; Mgt, magnetite; Mr, murashkoite; Po, pyrrhotite; Trv, trevorite, $NiFe_2O_4$; UN1 to UN6 – unknown phosphates and silicates (compositions are given in Table S1 in Supplementary Data).

Figure 2. Phosphide-troilite assemblages of the Cambria meteorite. (A) Fractured schreibersite grains (white with beige tint) in the matrix of microgranular troilite (tan-brown). Dark-gray: secondary iron hydroxides. Photomicrograph in reflected light. (B) Concentric phosphide assemblage in troilite matrix. The assemblage is composed of a pair of isometric grains of relict schreibersite (cores) replaced by a 5-10 μm onion-like barringerite-transjordanite shell. Photomicrograph in reflected light. (C) The same assemblage, false color BSE phase map. (D) Element concentrations across the profile depicted on (C). Note the steep Fe/Ni gradient across barringerite-transjordanite rim. Abbreviations: Tj, transjordanite; Br, barringerite; Schr, schreibersite; Tr, troilite; Fe-OH, secondary Fe hydroxides.

Figure 3. Calculated density plot for the minerals related to barringerite-transjordanite series. Black circles correspond to analyses of terrestrial Mo-free phosphides from the Hatrurim Formation. Red circles denote Mo-bearing compositions (Tables 1 and 6). Blue circles indicate (1) reference values for synthetic Fe_2P, Ni_2P and FeNiP (Fruchart et al. 1969), average density of the mineral from the

562 Cambria octahedrite (this work), and density of holotype barringerite from the Ollague pallasite
563 (Buseck 1969).
564
565 **Figure 4.** Ternary plots illustrating notable subordinate substitutions in the minerals related to the
566 barringerite-transjordanite series, in atoms per M_2P formula unit (*apfu*). (A) Fe-Ni plot for terrestrial
567 minerals with a statistics on Mo substitution. (B) Fe-Ni plot of phosphide rims in the Cambria
568 meteorite showing subordinate S content which substitutes for P.
569
570 **Figure 5.** Change of unit-cell parameters of terrestrial barringerite-transjordanite minerals along the
571 join Fe_2P–Ni_2P. The circles correspond to *a* parameter, the squares denote *c* parameter. The black
572 symbols relate to Mo-free minerals, the red ones mark Mo-bearing compositions. The blue graphs
573 trace the reference data for the synthetic Fe_2P–Ni_2P solid solutions (Fruchart et al. 1969). The input
574 analytical data are given in Tables 1 and 6.
575
576 **Figure 6.** Crystal structure of transjordanite (structure type Fe_2P). (A) Projection onto (0001). (B)
577 Projection close to $(1\bar{1}\bar{2}1)$. A framework built up of two types of infinite rods propagating along *c*
578 axis. The type 1 rods are composed of corner-sharing [$M(1)P_4$] tetrahedra (green), the type 2 rods are
579 represented by edge-sharing square pyramids [$M(2)P_5$] (yellow).
580
581
582

This is a preprint, the final version is subject to change, of the American Mineralogist (MSA)
Cite as Authors (Year) Title. American Mineralogist, in press.
DOI: https://doi.org/10.2138/am-2020-7275

583 **Tables**

584 **Table 1. Chemical composition of transjordanite-barringerite series minerals from the**
585 **localities of the Hatrurim Formation**
586

	Constituent (wt. %) [a]						Atoms per formula unit				
	Ni	**Fe**	**Co**	**Mo**	**P**	**Total**	**Ni**	**Fe**	**Co**	**Mo**	**P**
H01 [b]	78.10	1.30	0.66	-	20.39	100.45	1.97	0.03	0.02		0.98
H02	73.34	6.05	0.34	-	20.65	100.38	1.84	0.16	0.01		0.98
T03 [c]	67.80	10.20	-	-	21.50	99.50	1.72	0.27			1.02
H04	61.23	15.66	0.24	2.09	20.82	100.04	1.55	0.42		0.03	1.00
H05	52.16	25.28	0.10	1.47	20.66	99.67	1.32	0.67		0.03	0.99
H06	47.07	28.33	0.16	3.09	20.77	99.42	1.19	0.76		0.04	1.00
T07	29.23	49.97	-	-	21.34	100.54	0.72	1.28			0.99
H08	18.15	59.93	0.27	-	21.75	100.10	0.45	1.54			1.01
H09	12.66	64.61	0.09	1.86	21.15	100.37	0.32	1.67		0.03	0.98
H10	12.30	65.54	0.12	-	21.72	99.68	0.30	1.68			1.01
H11	9.46	69.39	0.13	-	21.60	100.58	0.23	1.77			1.00
T12	1.82	76.39	0.11	-	21.46	99.78	0.04	1.97			0.99

587
588 [a] The bar '-' denotes values below detection limit (~0.05 wt. %). The first letter in sample
589 abbreviations: H, Halamish wadi, Israel; T, Transjordan Plateau, Jordan (the type locality).
590 [b]Corresponds to a grain depicted on Fig. 1D. [c]The holotype specimen.
591
592
593
594

This is a preprint, the final version is subject to change, of the American Mineralogist (MSA)
Cite as Authors (Year) Title. American Mineralogist, in press.
DOI: https://doi.org/10.2138/am-2020-7275

Table 2. Chemical composition of transjordanite, barringerite and associated minerals from the Cambria meteorite [a]

	Tj	Br	Tj-Br	Schr	Tro	Km
	Wt. %					
Ni	60.55	17.62	32.93	23.37 (1.08)	-	4.21
Fe	18.16	60.02	45.51	61.09 (1.19)	62.28 (0.19)	95.70
Co	0.26	0.28	0.27 (0.06)	0.23 (0.05)	0.27 (0.09)	0.48
Cr	-	-	-	-	0.36 (0.05)	-
P	20.53	21.49	21.05 (0.25)	15.45 (0.16)	-	-
S	0.27	0.22 (0.19)	0.31 (0.19)	-	36.97 (0.18)	-
Total	99.77	99.63	100.07	100.14	99.88	100.39
	Atoms per formula unit (*apfu*)					
Σ *apfu*	3	3	3	4	2	1
Ni	1.52	0.43	0.81	0.80	-	0.040
Fe	0.48	1.58	1.18	2.19	0.978	0.955
Co	0.01	0.01	0.01	0.01	0.004	0.005
Cr	-	-	-	-	0.006	-
Σ	2.01	2.02	2.00	3.00	0.988	1.000
P	0.98	0.99	0.99	1.00	-	-
S	0.01	-	0.01	-	1.012	-
Σ	0.99	0.99	1.00	1.00	1.012	-

[a]Abbreviations: Tj, transjordanite, max. Ni content; Br, barringerite, max. Fe content; Tj-Br, average composition of transjordanite-barringerite aggregates; Schr, schreibersite, average of 33 analyses; Tro, troilite, average of 6 analyses; Km, "kamacite". Standard deviations (esd, wt. %) are given in parentheses. The bar '-' denotes values below detection limit (~0.05 wt. %).

This is a preprint, the final version is subject to change, of the American Mineralogist (MSA)
Cite as Authors (Year) Title. American Mineralogist, in press.
DOI: https://doi.org/10.2138/am-2020-7275

606 **Table 3. Crystal parameters, data collection, structure refinement details and bond**
607 **lengths for holotype transjordanite**
608

Crystal data	
Chemical formula	$(Ni_{1.73}Fe_{0.27})_{\Sigma=2.00}P$ [a]
Crystal size (mm)	0.08 × 0.06 × 0.05
Crystal system, space group	Hexagonal, $P\bar{6}2m$
a, c (Å), V (Å^3), Z	5.8897(3), 3.3547(2), 100.78(1), 3
D_x (g/cm^3)	7.297
Data collection and refinement	
Instrument	Bruker APEX DUO (CCD detector)
X-ray source and optics	Mo$K\alpha$, microfocus tube, 50 kV, 0.60 mA
2Θ range (°)	8.0–70.0 (truncated at 70 °)
No. of measured, independent and observed [$I > 2\sigma(I)$] reflections	3524, 192, 190
h, k, l range	–9→9, –9→9, –5→5
R_{int}, R_σ	0.057, 0.022
R_1 ($\|F_o\| \geq 4\sigma_F$), wR_2, S=GoF	0.013, 0.024, 1.156
$\Delta\sigma_{min}$, $\Delta\sigma_{max}$ (e/Å^3)	–0.57, 0.47
Bond lengths (Å)	
M(1)—P1	2.2080(4) × 2
M(1)—P2	2.2744(4) × 2
M(2)—P1	2.4622(2) × 4
M(2)—P2	2.3464(7)

609
610 [a] Determined by the site occupancy refinement.
611
612

This is a preprint, the final version is subject to change, of the American Mineralogist (MSA)
Cite as Authors (Year) Title. American Mineralogist, in press.
DOI: https://doi.org/10.2138/am-2020-7275

Table 4. Fractional atomic coordinates and displacement parameters (Å^2) for holotype transjordanite

Site [a]	*x*	*y*	*z*	U_{iso}	U^{11}	U^{22}	U^{33}	U^{12}
M(1) (3*f*) [b]	0.73920(9)	0	0	0.00727(15)	0.0062(2)	0.0064(2)	0.0093(2)	0.00318(12)
M(2) (3*g*)	0.39839(11)	0	1/2	0.01063(17)	0.0089(2)	0.0157(3)	0.0095(2)	0.00785(14)
P1 (2*c*)	2/3	1/3	0	0.0075(2)	0.0058(3)	0.0058(3)	0.0107(5)	0.00292(15)
P2 (1*b*)	0	0	1/2	0.0067(3)	0.0066(4)	0.0066(4)	0.0070(6)	0.0033(2)

[a]Site multiplicities and Wyckoff symbols are given in parentheses. [b]Metal site occupancies: *M*(1), ($Ni_{0.73}Fe_{0.27}$); *M*(2), $Ni_{1.00}$. U^{13} and U^{23} are equal to 0 by default.

This is a preprint, the final version is subject to change, of the American Mineralogist (MSA)
Cite as Authors (Year) Title. American Mineralogist, in press.
DOI: https://doi.org/10.2138/am-2020-7275

623 **Figures**
624

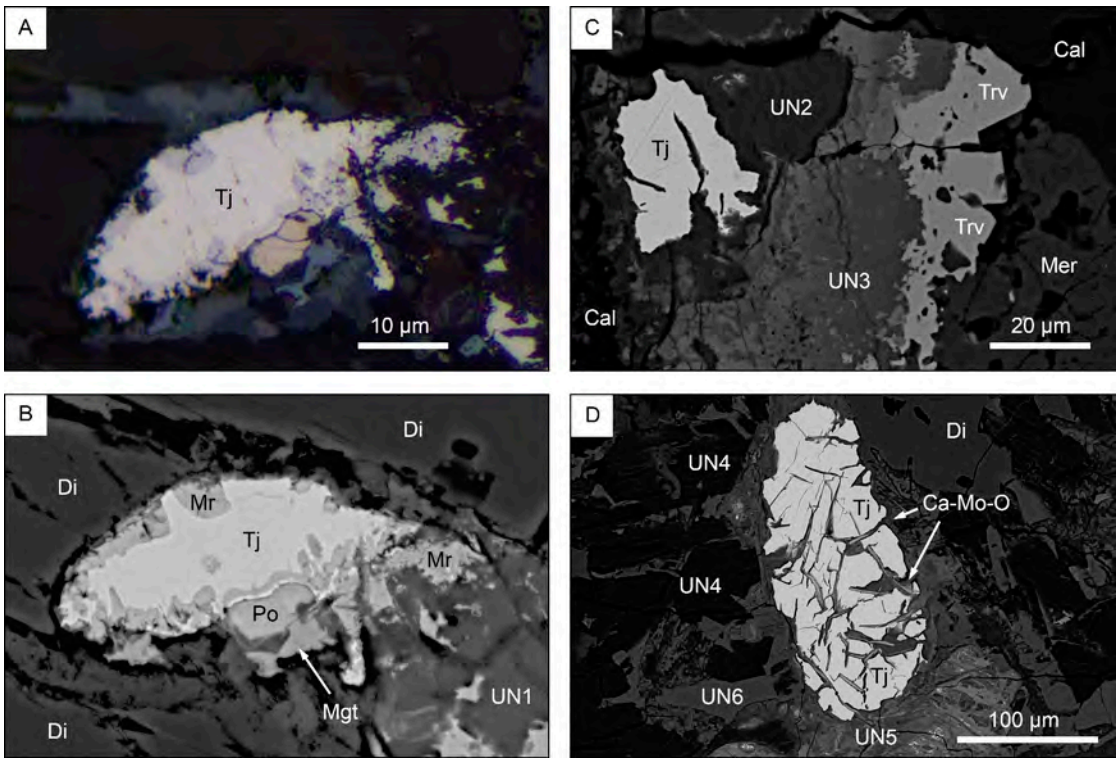

625

626 **Figure 1**

627

628

629

630

This is a preprint, the final version is subject to change, of the American Mineralogist (MSA)
Cite as Authors (Year) Title. American Mineralogist, in press.
DOI: https://doi.org/10.2138/am-2020-7275

631

632

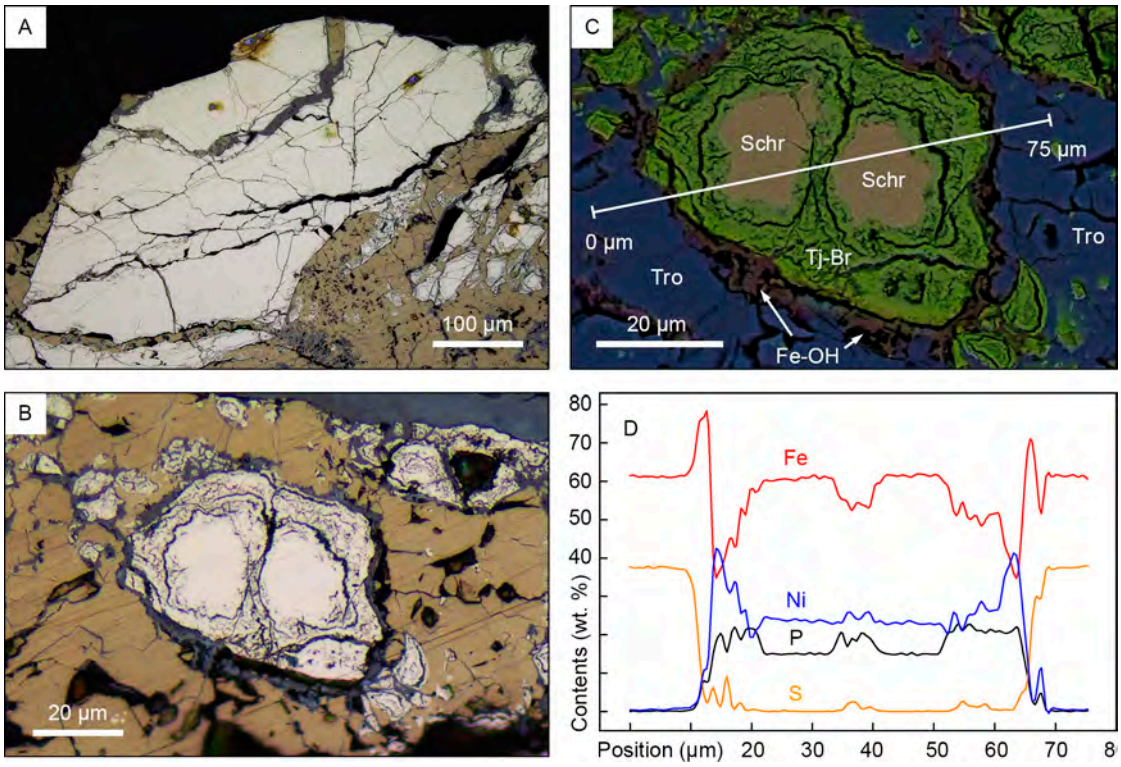

633

634 **Figure 2**

635

636

637

638

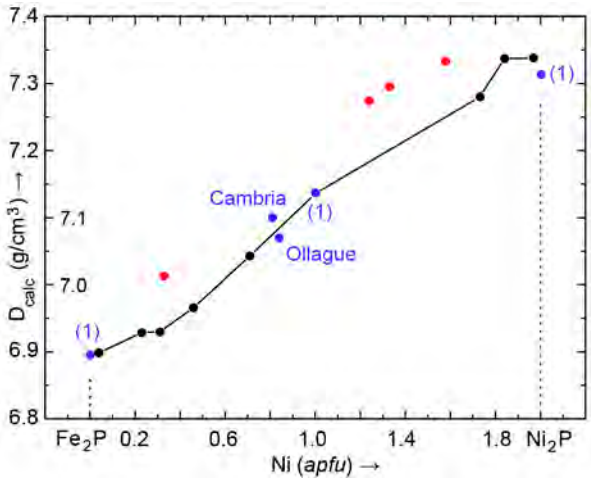

639

640 **Figure 3**

641

642

This is a preprint, the final version is subject to change, of the American Mineralogist (MSA)
Cite as Authors (Year) Title. American Mineralogist, in press.
DOI: https://doi.org/10.2138/am-2020-7275

643

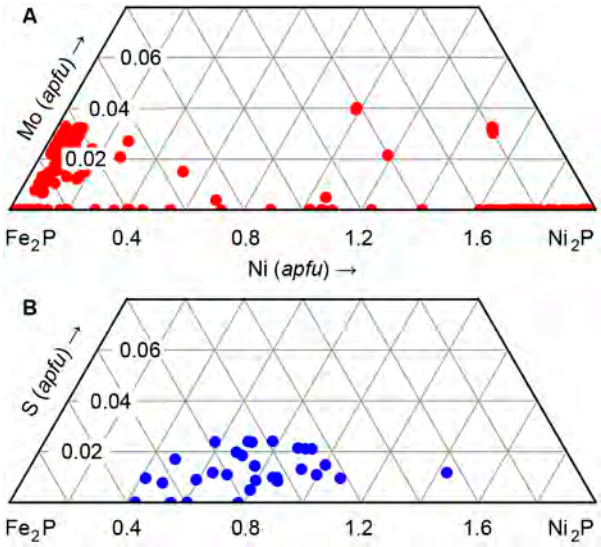

644

645

646 **Figure 4**

647

648

649

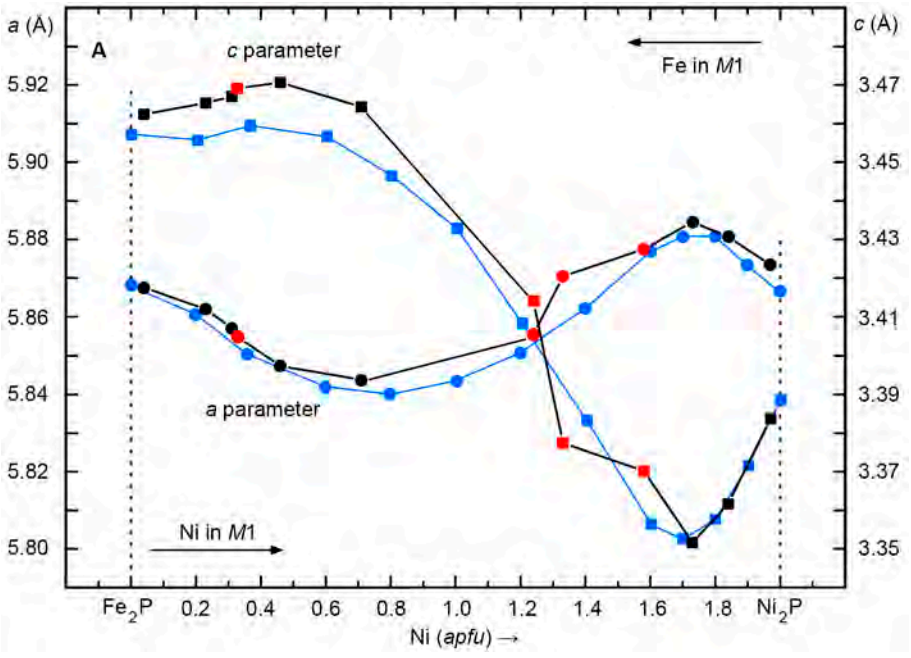

650

651 **Figure 5**

652

653

This is a preprint, the final version is subject to change, of the American Mineralogist (MSA)
Cite as Authors (Year) Title. American Mineralogist, in press.
DOI: https://doi.org/10.2138/am-2020-7275

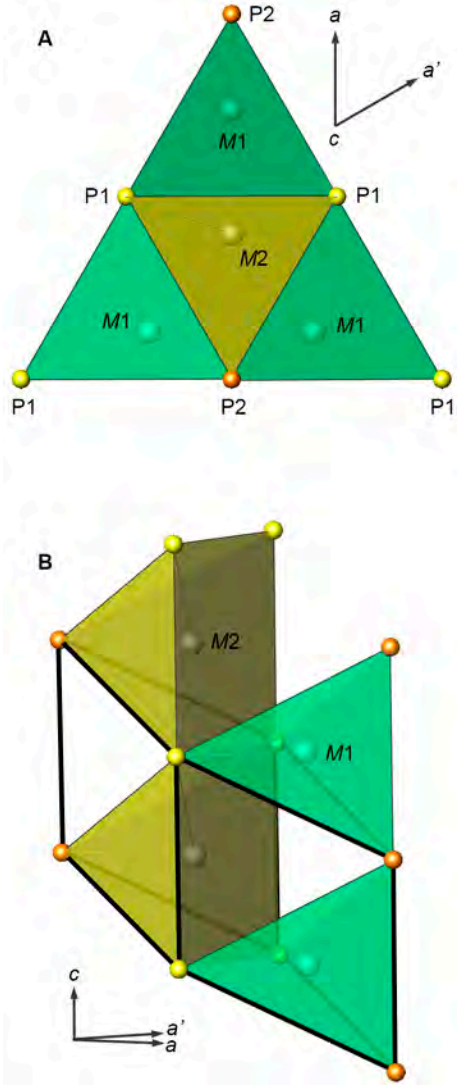

Figure 6